

Pericyte loss initiates microvascular dysfunction in the development of diastolic dysfunction

Steven J. Simmonds^{1,†}, Mandy O.J. Grootaert^{1,†}, Ilona Cuijpers^{1,2,†}, Paolo Carai¹, Nadeche Geuens¹, Melissa Herwig^{3,4,5}, Pieter Baatsen^{6,7}, Nazha Hamdani ^{3,4,5}, Aernout Luttun¹, Stephane Heymans^{1,2,†}, and Elizabeth A.V. Jones ^{1,2,*†}

¹Centre for Molecular and Vascular Biology, KU Leuven, Herestraat 49, bus 911, Leuven 3000, Belgium; ²Department of Cardiology, Maastricht University, CARIM School for Cardiovascular Diseases, Universiteitssingel 50, Maastricht 6229 ER, The Netherlands; ³Department of Cellular and Translational Physiology, Institute of Physiology, Ruhr University Bochum, Bochum 44801, Germany; ⁴Molecular and Experimental Cardiology, Institut für Forschung und Lehre (IFL), Ruhr University Bochum, Bochum, Germany; ⁵Department of Cardiology, St.Josef-Hospital, Ruhr University Bochum, Bochum, Germany; ⁶VIB-KU Leuven, Center for Brain and Disease Research, Electron Microscopy Platform & VIB Bioimaging Core, Leuven, Belgium; and ⁷Department of Neurosciences, Leuven Brain Institute, KU Leuven, Leuven, Belgium

Received 4 August 2023; revised 27 November 2023; accepted 30 November 2023; online publish-ahead-of-print 9 December 2023

Handling Editor: Daniel FJ Ketelhuth

Aims

Microvascular dysfunction has been proposed to drive heart failure with preserved ejection fraction (HFpEF), but the initiating molecular and cellular events are largely unknown. Our objective was to determine when microvascular alterations in HFpEF begin, how they contribute to disease progression, and how pericyte dysfunction plays a role herein.

Methods and results

Microvascular dysfunction, characterized by inflammatory activation, loss of junctional barrier function, and altered pericyte–endothelial crosstalk, was assessed with respect to the development of cardiac dysfunction, in the Zucker fatty and spontaneously hypertensive (ZSF1) obese rat model of HFpEF at three time points: 6, 14, and 21 weeks of age. Pericyte loss was the earliest and strongest microvascular change, occurring before prominent echocardiographic signs of diastolic dysfunction were present. Pericytes were shown to be less proliferative and had a disrupted morphology at 14 weeks in the obese ZSF1 animals, who also exhibited an increased capillary luminal diameter and disrupted endothelial junctions. Microvascular dysfunction was also studied in a mouse model of chronic reduction in capillary pericyte coverage (*PDGF-B^{ret/ret}*), which spontaneously developed many aspects of diastolic dysfunction. Pericytes exposed to oxidative stress *in vitro* showed downregulation of cell cycle-associated pathways and induced a pro-inflammatory state in endothelial cells upon co-culture.

Conclusion

We propose pericytes are important for maintaining endothelial cell function, where loss of pericytes enhances the reactivity of endothelial cells to inflammatory signals and promotes microvascular dysfunction, thereby accelerating the development of HFpEF.

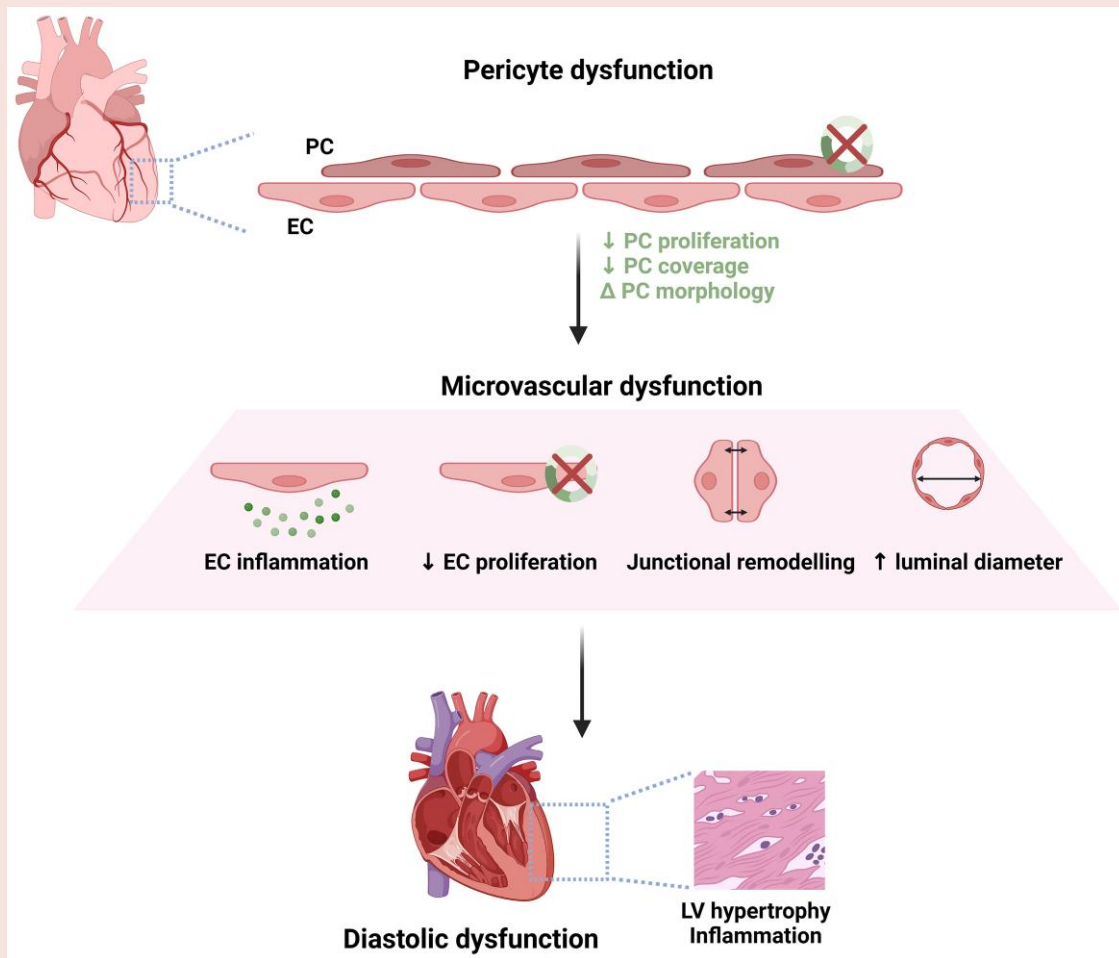
* Corresponding author. Tel: +32 16 32 93 62, Email: liz.jones@kuleuven.be

† The first three authors and the last two authors contributed equally to the study.

© The Author(s) 2023. Published by Oxford University Press on behalf of the European Society of Cardiology.

This is an Open Access article distributed under the terms of the Creative Commons Attribution-NonCommercial License (<https://creativecommons.org/licenses/by-nc/4.0/>), which permits non-commercial re-use, distribution, and reproduction in any medium, provided the original work is properly cited. For commercial re-use, please contact journals.permissions@oup.com

Graphical Abstract



Keywords

Microvascular dysfunction • Metabolic comorbidities • Pericytes • HFpEF

Introduction

More than half of the heart failure (HF) patients suffer from HF with preserved ejection fraction (HFpEF), a complex cardiovascular syndrome characterized by cardiac inflammation, fibrosis, cardiomyocyte hypertrophy, and endothelial dysfunction.¹ Heart failure with preserved ejection fraction is strongly associated with the presence of metabolic comorbidities (e.g. type 2 diabetes mellitus, obesity, and hypertension).² The current paradigm is that these systemic factors induce chronic inflammation and endothelial cell dysfunction, driving microvascular dysfunction and disease progression.² Microvascular dysfunction is a combination of structural remodelling of the microvasculature, endothelial cell-associated dysfunction, and/or mural cell dysfunction.³ While it is well studied in ischaemic cardiovascular diseases, its role in HFpEF remains unclear. Recent insights show that the majority of HFpEF patients present with coronary microvascular dysfunction.⁴ Additionally, it has been established that HFpEF patients have a reduced coronary flow reserve, a proxy for coronary microvascular dysfunction that increases the risk of hospitalization more than five-fold.^{5,6} Another study showed that HFpEF patients develop a reduced cardiac capillary

density, called microvascular rarefaction.⁷ These findings indicate that changes in the microcirculation are part of HFpEF development, but as yet the paradigm that they are causative in the disease has not been tested. Though the endothelium has been the main focus of research into microvascular dysfunction in HFpEF, the microvasculature is composed not only of endothelial cells but also of other cell types such as pericytes. Pericytes have been shown to play a significant role in controlling endothelial cell physiology.⁸ Pericytes communicate with endothelial cells through gap junctions and by secreting growth factors.⁸ Because of their role in dementia, research has focused primarily on brain pericytes, where they have been shown to affect microvascular flow.^{9,10} Pericytes also control brain permeability¹¹ and affect immune responses.¹² In contrast, the role of cardiac pericytes has been little studied.

To study the microvascular changes during the development of left ventricle diastolic dysfunction, we used the ZSF1 obese rat.^{13,14,15,16} Here, we show that cardiac pericyte coverage is reduced in the obese ZSF1 rat before prominent echocardiographic signs of diastolic dysfunction are present. Furthermore, in the *PDGF-B^{ret/ret}* mutation model of pericyte loss, we observed the development of diastolic dysfunction

in the absence of other stimuli. Pericytes are essential for maintaining vascular integrity, permeability, and tone.^{17,18} We show here that the pericytes exposed to oxidative stress induced a pro-inflammatory state in endothelial cells. Our data suggest a protective role for cardiac pericytes in microvascular dysfunction during the development of diastolic dysfunction.

Methods

Experimental animal studies

Experiments were performed according to the European Directive on the Care and Use of Experimental Animals (2010/63/EU) and approved by the Animal Care and Use Committee of KU Leuven (Projects 178/2016 and 116/2021). Male obese ZSF1 rats and lean control littermates were obtained at the youngest age possible (5 weeks) from Charles River Laboratories (#379 and 378, respectively). Female and male *PDGF-B^{ret/ret}* mice and littermate *PDGF-B^{ret/+}* controls were analysed at 12 and 27 weeks of age.¹⁹ Both rats and mice were housed and acclimated under a 14-h light–10-h dark cycle with access to water and chow diet *ad libitum* (V1534-000, Sniff Spezialdiäten GmbH).

Blood pressure and fasting glucose measurements

At 6, 14, and 21 weeks of age, the blood pressure of lean and obese conscious ZSF1 rats ($n = 7/\text{group}$) was assessed using the CODA tail-cuff system (Kent Scientific). Blood pressure was assessed at 12 and 27 weeks of age in *PDGF-B^{ret/ret}* and *PDGF-B^{ret/+}* mice, 2 days prior to sacrifice. For seven days before the measurements, animals were placed in the restrainer between 5 and 15 minutes to acclimatize. On the day of measurement, the tail cuff was placed on the animals and 10 cycles were recorded to acclimatize the animal, followed by at least 10 cycles for analysis. To assess fasting glucose levels, lean and obese ZSF1 rats ($n = 12/\text{group}$) were fasted for 16 h, placed in the restrainer, and glucose levels were assessed via tail vein puncture with Glucomen LX Plus (A. Menarini Diagnostics).

Transthoracic echocardiography

At each time point, ZSF1 lean ($n = 9$) and obese ($n = 11$) rats were anaesthetized with 50 mg/kg ketamine (Nimatek, Eurovet Animal Health BV) and 5 mg/kg xylazine (Xyl-M) dissolved in 0.9% saline. *PDGF-B^{ret/ret}* and *PDGF-B^{ret/+}* animals were anaesthetized using 3% inhaled isoflurane (Ecuphar NV) for induction followed by 1% inhaled isoflurane for maintenance. Transthoracic echocardiography was performed as previously described.¹³ In brief, a MS 250 transducer (13–24 MHz) connected to a Vevo 2100 echocardiograph (Visual Sonics) was used for rats whereas a MX550D transducer (55 MHz) connected to a Vevo 3100 echocardiograph was used for mice. Animals were placed in a supine position on a heating pad to maintain the core body temperature between 37.5°C and 37.7°C, measured by a rectal probe. Heart rate, left ventricular internal diameter, posterior wall thickness, and anterior wall thickness were assessed by parasternal short-axis M-mode imaging. Stroke volume, ejection fraction (EF), fractional shortening, left ventricular volumes, and end-diastolic and end-systolic volume (Teichholz formula) were calculated based on parasternal short-axis M-mode recordings. Left ventricular filling was assessed by pulsed wave Doppler trans-mitral flow velocity tracings, including early and late mitral inflow peak velocity (E and A' , respectively), mitral valve deceleration time (MV DT), isovolumetric relaxation time (IVRT), non-flow time (NFT), aortic ejection time, and isovolumetric contraction time, just above the tip of the mitral leaflets, and myocardial perfusion index was calculated. Myocardial movements and early and late diastolic mitral annulus peak velocity (E' and A' , respectively) were measured by tissue Doppler imaging at the lateral mitral annulus. E/A , MV DT, and E/E' ratios were calculated. At least three stable cardiac cycles were averaged for all measurements.

Organ collection

At each time point, lean ($n = 7$ except at 6 weeks) and obese ($n = 7$) ZSF1 rats were anaesthetized by intraperitoneal injection of 50 mg/kg ketamine and 5 mg/kg xylazine dissolved in 0.9% NaCl. *PDGF-B^{ret/+}* and *PDGF-B^{ret/ret}*

animals ($n = 6/8$ at 12 weeks, $n = 14/14$ at 27 weeks, for *PDGF-B^{ret/+}* and *PDGF-B^{ret/ret}*, respectively) were anaesthetized by intraperitoneal injection of 100 mg/kg ketamine and 10 mg/kg xylazine dissolved in 0.9% NaCl. Blood was collected from the abdominal aorta in EDTA, centrifuged for 10 min at 13 000 rpm, and then plasma was collected and stored at -80°C for future analysis. Animals were then perfused with 20 mL phosphate buffered saline (PBS) by inserting a butterfly needle in the left ventricle, while making a cut in the right atrium. Animals were euthanized by excision of the heart, and organs were collected and weighed. Organ weights were normalized by tibia length (TL).

Cardiac histology

An approximately 5 mm section of the heart was fixed in 4% paraformaldehyde at 4°C for 24 h and embedded in paraffin. Another equally sized section was flash frozen in liquid nitrogen. Paraffin-embedded 4 μm sections were used for Picro Sirius Red and Laminin A (Sigma Aldrich L9393, 1/400) stainings. The amount of total and perivascular cardiac fibrosis was quantified as the percentage Sirius Red positive area per total and perivascular area, respectively. Interstitial fibrosis (total minus perivascular fibrosis) was expressed as percentage of total fibrosis. The largest diameter of the fibrotic tissue in the tunica adventitia (perivascular fibrosis thickness) around each vessel diameter class was quantified. Cardiomyocyte hypertrophy was assessed by calculating the myocyte cross-sectional area based on the inner circumference of at least 100 cardiomyocytes per laminin-stained section. Frozen cardiac tissue (10 μm) was used for VE-Cadherin (R&D, AF1002, 1/50), Ki-67 (EpreDia, RB1510P1, 1/50), Isolectin GS-IB₄ (Thermo Fisher, I21411, 1/50), neuron glial antigen 2 (NG2, EMD Millipore, Ab5320, 1/100), and alpha smooth muscle actin (α -SMA, Sigma-Aldrich, C6198, 1/200). All secondaries were used at a concentration of 1/400 and were AlexaFluor conjugated, except for laminin that was horse radish peroxidase conjugated and used at a concentration of 1/100. Pericyte coverage was determined by counting the number of capillary vessels (isolectinB4+) that are covered by NG2+ cells. Capillary vessels are defined as vessels smaller than 10 μm in diameter. Twenty-micrometre-thick frozen sections were used to evaluate the jaggedness of junctions on a VE-Cadherin staining. Three to five images were taken per animal, and all individual files were renamed to hide both the genotype and which animal they belonged to. These were then evaluated blindly by an independent observer. The VE-Cadherin junctions were scored as either 'straight' (score 1) or 'jagged' (score 3). Then, the median of all images per animal was calculated. We then counted how many mice were scored 1, 2, or 3. Next, chi square was used to calculate the distribution and its significance per group. All fluorescent images were taken with a Zeiss 700M confocal microscope. All bright field images were taken on Zeiss Axiovert 200M, equipped with AxioCam Mrc5 colour camera. Images were analysed using ImageJ (NIH).

Measurement of circulating interleukin levels

Circulating levels of interleukin-1 beta (IL1B) and interleukin 6 (IL6) in plasma of ZSF1 rats were measured using the rat IL1B Quantikine ELISA Kit (RLB00) and the rat IL6 Quantikine ELISA Kit (R6000B), respectively. Interleukin-1 alpha (IL1A) was determined using the rat IL1A Quantikine ELISA Kit (RRA00) but was below the limit of detection and thus not reported.

Culturing of pericytes

Immortalized human pericytes from a male donor (Celther, CL 05008-CLTH) were cultured in DMEM (Thermo Fisher, 41965039) supplemented with penicillin/streptomycin and 10% foetal bovine serum (FBS). To mimic oxidative stress, pericytes were stimulated with or without 100 μM H_2O_2 with one media change after 12 h (Sigma-Aldrich, H1009).²⁰ Cells were collected for RNA or a Ki67 staining to assess proliferation. For the Ki67 staining, cells were grown on coverslips, fixed in 4% PFA for 10 min and then permeabilized with 0.3% triton X-100 at room temperature (RT) for 20 min. Next, cells are washed and blocked in 3% bovine serum albumin (BSA) (in PBS) at RT for 1 h. Then, cells are incubated with anti-mouse/rat Ki-67 antibody (1/100 dilution in 0.1% BSA) at overnight at 4°C on a shaker. Next day, cells are washed, and incubated with anti-rat Alexa fluor 568 for 1 h at RT. Then, cells are washed, stained with DAPI,

mounted on glass slides, and imaged. Four images per sample were taken, and the % proliferation was averaged per sample.

RNA sequencing and data analysis

Pericytes (100 μ M H₂O₂-treated for 24 h with media change every 8 h or control cells) were collected for RNA sequencing (RNA-seq). All agents were diluted in media supplemented with penicillin/streptomycin and 2% FBS. The RNA-seq was performed by the Genomics Core (KU Leuven, Belgium). Sequence libraries were prepared with the Lexogen QuantSeq 3' mRNA-Seq Library Prep Kit according to the manufacturer's protocol. Samples were indexed to allow for multiplexing. Library quality and size range were assessed using a Bioanalyzer with the DNA 1000 Kit (both Agilent Technologies) according to the manufacturer's recommendations. Libraries were diluted to a final concentration of 2 nM and subsequently sequenced on an Illumina HiSeq4000 platform. Single-end reads of 50 bp length were produced with a minimum of 1 M reads per sample. Quality control of raw reads was performed with FastQC v0.11.7. Adapters were filtered with ea-utils fastq-mcf v1.05. Splice-aware alignment was accomplished using HISAT2 (<http://daehwankimlab.github.io/hisat2/>) against the human reference genome hg38 using the default parameters. Reads mapping to multiple loci in the reference genome were discarded. The resulting BAM alignment files were handled with SAMtools v1.5. Reads per gene were quantified by HT-seq Count v2.7.14. Count-based differential expression analysis was assessed with R-based (The R Foundation for Statistical Computing, Austria) Bioconductor package DESeq2. *P*-values were adjusted for multiple testing with the Benjamini–Hochberg procedure, which controls false discovery rate. Differentially expressed genes in pericytes exposed to oxidative stress vs. controls (adjusted *P* < 0.05) were presented in heatmaps. Pathway analysis was performed using Reactome. The RNA-seq data set can be found in the Gene Expression Omnibus repository; accession number GSE251995.

Real-time quantitative polymerase chain reaction

RNA was extracted from cells using the Qiagen RNeasy Mini Kit (74104) or from heart tissue using the Qiazol Lysis Reagent (79306). RNA was converted into cDNA using M-MLV reverse transcriptase (Promega, M1701). Real-time quantitative polymerase chain reaction (qPCR) was performed using SYBR Green PCR master mix (Thermo Fisher, 4364344) on an Applied Biosystems qPCR device. All primer sequences are listed in [Supplementary material online, Table S1](#). Data were normalized to house-keeping genes RPL13A (human) and RPL32A (rat).

Co-culture of pericytes and endothelial cells

Pericytes (100 μ M H₂O₂ treated for 24 h with one media change after 12 h or control cells) were co-cultured with human umbilical vein endothelial cells (HUVECs) in transwell inserts (Corning, 353095, 0.4 μ m pore size) preventing direct cell–cell contact. H₂O₂-treated (or control) pericytes were seeded in the inserts (20 000 cells/insert), and endothelial cells (30 000 cells/well) were seeded on the bottom of the well. Pericytes and endothelial cells were co-cultured for 2 days, followed by a treatment with human TNF α (1 ng/mL, Peprotech 300-01A) for 8 h.

Transmission electron microscopy

Samples were fixed in 4% paraformaldehyde and 2.5% glutaraldehyde (both from Electron Microscopy Sciences) in 0.1 M sodium cacodylate buffer, and after washing in the same buffer, subsequently treated with 1% osmium tetroxide (Electron Microscopy Sciences) and 1.5 mM ferrocyanide in 0.1 M sodium cacodylate buffer. Then, after washing in 0.1 M cacodylate buffer, the samples were stained *en bloc* with 1% uranyl acetate (SPI Supplies) and lead aspartate.²¹ Finally, the samples were rinsed and dehydrated in a graded ethanol series from 30% to 100% after which they were washed in propylene oxide and embedded in epoxy resin. Ultrathin sections (70 nm) were cut with a Leica ultracut S ultramicrotome and some of them post-stained in uranyl acetate and Reynold's lead citrate. The sections were examined, and images were taken with a JEOL JEM1400 transmission electron microscope equipped with an 11 Mpxl EMSIS Quemesa camera.

Ten to thirteen images were taken per animal blindly by an independent researcher.

Statistical analysis

Results are presented as mean \pm SEM. Statistical analysis was performed using GraphPad software V8. ROUT testing was performed, and statistical outliers removed were applicable. Data with three groups or more were analysed using a two-way analysis of variance (ANOVA) with Sidak's comparison *post hoc* test. Data with two groups were analysed using a two-tailed unpaired Student's *t*-test or a Mann–Whitney *U* test for non-parametric testing. Statistical significance for the scores of jaggedness was analysed with a Pearson chi-squared test. *P*-values of <0.05 were considered statistically significant.

Results

Metabolic risk factors, diastolic dysfunction, and cardiac tissue dysfunction in the obese ZSF1 rat heart failure with preserved ejection fraction model

To characterize the obese ZSF1 rat model, we assessed their metabolic risk factors, cardiac function, and cardiac histology at 6, 14, and 21 weeks of age vs. their lean counterparts. Obese ZSF1 rats had increased body weight ([Figure 1A](#)) at 6 weeks compared with lean rats. Both lean and obese ZSF1 rats displayed hypertension (systolic and diastolic blood pressure of >129 and 91 mm Hg, respectively) at all stages ([Figure 1B](#); [Supplementary material online, Table S2](#)). Hyperglycaemia (fasting glucose > 7 mM) was only seen as of 14 weeks in the obese ZSF rats ([Figure 1C](#)). Cardiac function was assessed using echocardiography. Some diastolic parameters changed as early as 14 weeks of age in ZSF1 obese rats (i.e. MV DT and IVRT), but many characteristics of diastolic dysfunction were only observed at 21 weeks of age, reflected by an increased deceleration time, IVRT, NFT, *E'* (mitral annular velocity), and reduced *E/A* ratio [ratio of early passive filling of the left ventricle (*E*), to late active filling (*A*)] ([Figure 1D–H](#); [Supplementary material online, Table S2](#)). Systolic function was preserved in lean and obese ZSF1 rats at all time points, reflected by a preserved EF (>50%, [Figure 1I](#); [Supplementary material online, Table S2](#)). In our hands, the ZSF1 phenotype at 21 weeks appears to be one of pre-HFpEF. Our data agree with a previous timeline by Hamdani et al.¹⁴ of HFpEF development in this animal model, but not that published by Schauer et al.,¹⁶ who indicate earlier development of the cardiac phenotype.

Heart failure with preserved ejection fraction occurs because the heart becomes stiffer and larger, a process involving both the extracellular matrix production and cardiomyocyte hypertrophy as a compensatory change to increased cardiomyocyte stiffness.²² Both total and interstitial fibrosis were similar in lean and obese ZSF1 rats at all time points; however, perivascular fibrosis was significantly increased around mid-sized (diameter < 76 μ m) and larger (76–100 μ m) cardiac vessels in obese ZSF1 rats at 21 weeks ([Figure 1J and K](#); [Supplementary material online, Figure S1](#)). Cardiomyocyte cross-sectional area was increased in obese ZSF1 rats at both 14 and 21 weeks ([Figure 1L and M](#)), with an increase in heart weight (normalized to TL) at 21 weeks ([Figure 1N](#)).

The microvascular milieu is disrupted before diastolic dysfunction develops

We next investigated microvascular changes in relation to the development of diastolic dysfunction. We observed a reduction in capillary density at the 21-week stage ([Figure 2A](#)), when significant diastolic dysfunction is already established in these animals. However, pericyte coverage was already decreased at 14 weeks (41% reduction,

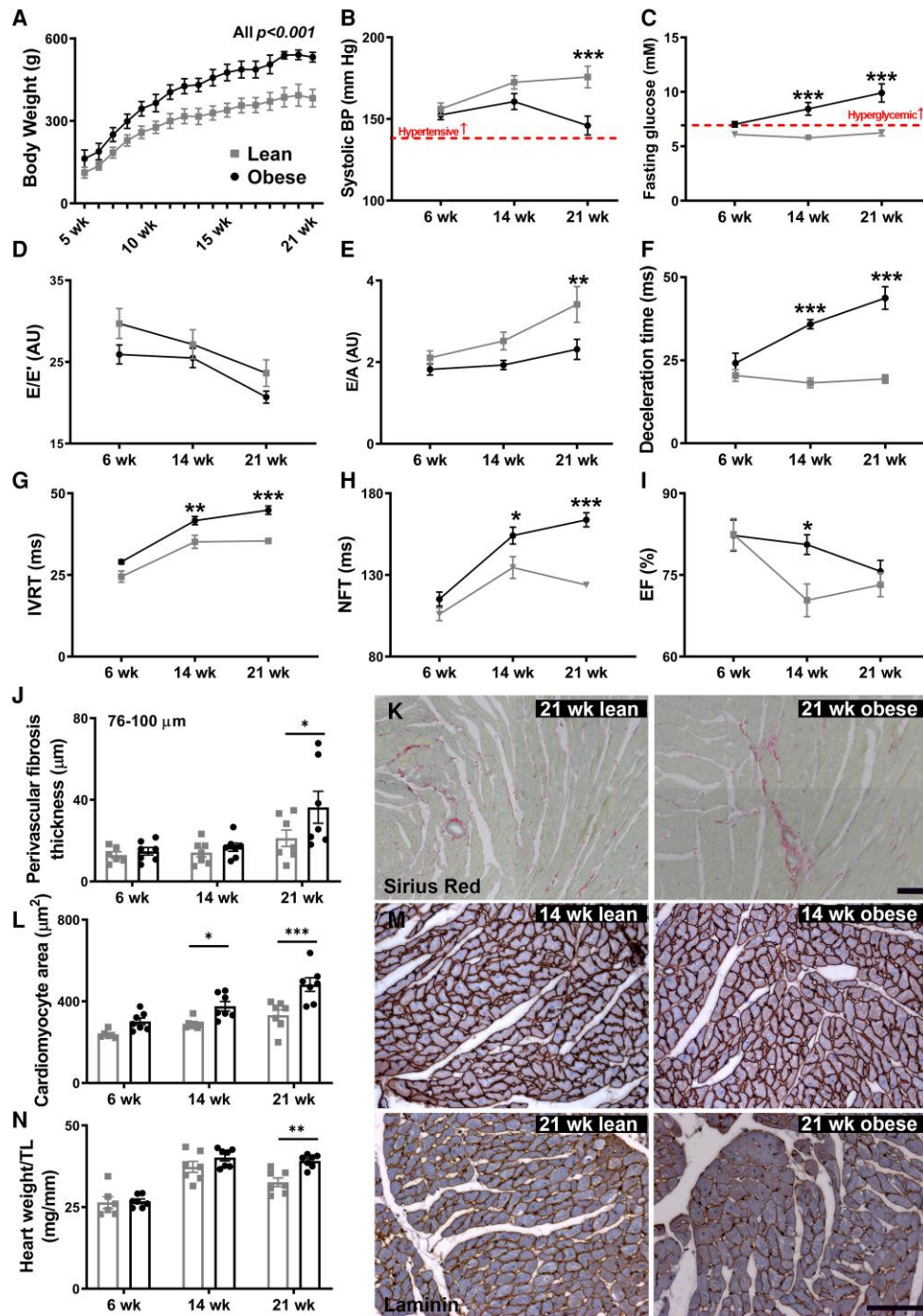


Figure 1 Metabolic risk factors develop early in obese ZSF1 rats, while many histological and echocardiographic signs of heart failure with preserved ejection fraction are not present until 21 weeks of age. Body weight (A; $n = 11/\text{group}$), systolic blood pressure (B, $n = 7/\text{group}$), and fasting glucose levels (C; $n = 12/\text{group}$) were analysed to establish when metabolic risk factors for heart failure with preserved ejection fraction develop in the ZSF1 rat model. E/E' ratio (D), E/A ratio (E), deceleration time (F), isovolumetric relaxation time (G), non-flow time (H), and ejection fraction (I) were used to establish when heart failure with preserved ejection fraction could be detected by echocardiography in lean ($n = 9$) and obese ($n = 11$) ZSF1 rats. Cardiac Sirius Red staining to assess perivascular fibrosis in large (76–100 μm) vessels with representative image at 21 weeks (J and K; $n = 7/\text{group}$). Cardiac laminin staining was used to measure cardiomyocyte cross-sectional area with representative image at 14 and 21 weeks (L and M; $n = 7/\text{group}$). The heart weight to TL in obese and lean ZSF1 rats was also evaluated as a sign of hypertrophy (N; $n = 7/\text{group}$). Scale bars are 100 μm (K and M) and apply to all images within a panel. Values are presented as mean \pm SEM. Significance is assessed by a non-paired two-way ANOVA followed by Sidak's multiple comparisons test with $*P < 0.05$, $**P < 0.01$, and $***P < 0.001$. A, late mitral inflow peak velocity; E, early mitral inflow peak velocity; E' , early diastolic annulus peak velocity; EF, ejection fraction; IVRT, isovolumetric relaxation time; NFT, non-flow time; TL, tibia length.

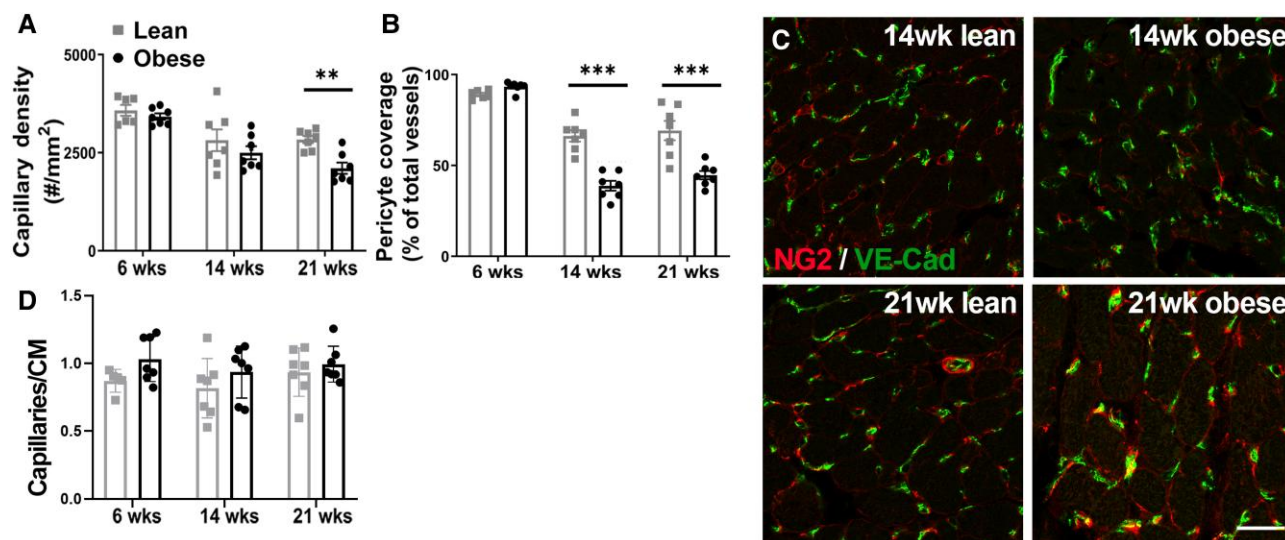


Figure 2 Pericyte loss is present in ZSF1 rats before diastolic dysfunction develops. Quantification of vascular density, based on VE-Cadherin staining indicates that vascular density is only decreased at the 21-week stage in ZSF1 obese rats as compared with lean ZSF1 rats (A; $n = 7/\text{group}$). Pericyte coverage, assessed by NG2+ cells localized to IB4+ capillary-sized vessels, was reduced from the 14-week stage onwards (B and C; $n = 7/\text{group}$). Representative images are shown at 14 and 21 weeks. Average number of capillary vessels per cardiomyocyte (CM) was calculated by multiplying the capillary density by the average cardiomyocyte size per heart (D; $n = 7/\text{group}$).

Figure 2B and C; Supplementary material online, Figure S2A and B) and remained reduced at 21 weeks (35% reduction). Therefore, the pericyte dysfunction preceded the onset of diastolic dysfunction. Furthermore, when calculating the average number of capillaries per cardiomyocyte, no changes in vascular density were present at any time point (Figure 2D).

Since microvascular dysfunction was present from 14 weeks onwards, we further studied pericyte and endothelial cell proliferation and pericyte morphology at the microvascular niche. Cardiac pericytes displayed reduced proliferation in obese ZSF1 rats at both the 14- and 21-week stages (Figure 3A and B; Supplementary material online, Figure S2C); however, cardiac endothelial cells did not show altered proliferation until the 21-week stage (Figure 3A and B). Pericyte morphology in obese ZSF1 rats at the 14-week stage was changed, with the remaining pericytes in the obese ZSF1 rat appearing more rounded (Figure 3C).

Pericytes form finger-like extensions believed to regulate tone in brain capillaries.²³ In the ZSF1 lean rats, pericytes had extensions that were only slightly smaller than the cell body. The pericytes in ZSF1 obese rats had either no extension or had a single very thin extension.

Pericyte morphology is important for maintaining capillary structure, so we next investigated changes in both capillary diameter and junctional disruption. ZSF1 obese rats at the 14-week stage showed an increase in cardiac capillary luminal diameter compared with lean rats, suggestive of capillary dilatation (Figure 3D and E). This was coupled with an increase of ‘jagged’ disassembled VE-Cadherin junctions (Figure 3F and G) reflecting the junctional changes that occur during microvascular remodelling events.^{24,25} Jagged junctions were present at the 14-week stage and sustained at the 21-week stage. To further investigate this, we used transmission electron microscopy to focus on endothelial junctions in the 14-week ZSF1 rats. We saw further evidence of endothelial junctional disruption, observing in the obese ZSF1 rats that endothelial junctions were wider at their max point, and there was a trend to an increased overall junctional area (Figure 3H and I).

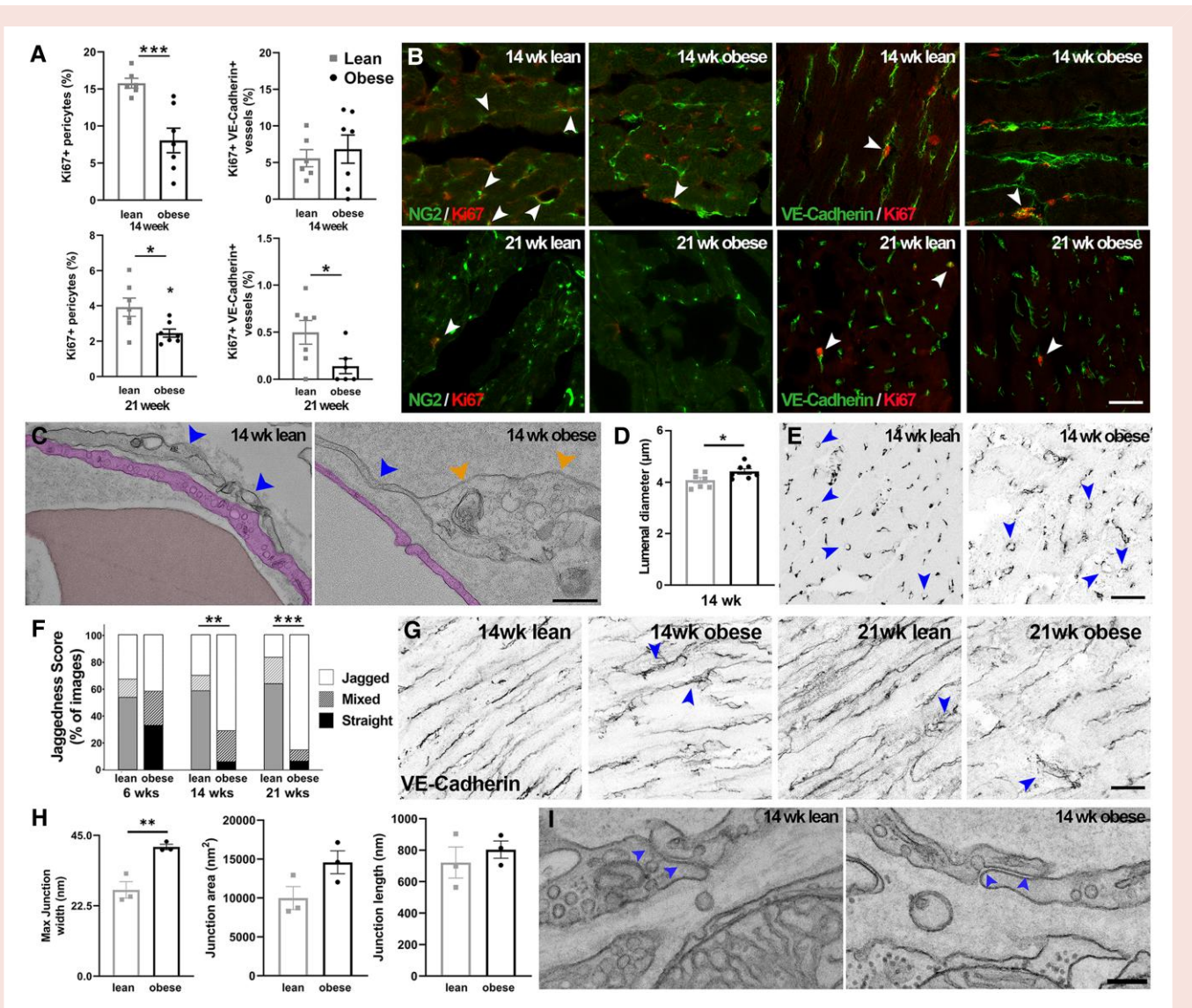
Finally, we determined the arteriolar density and vascular smooth muscle cell coverage to look for any structural changes to the larger vessels. Both cardiac density and average diameter of $\alpha\text{-SMA}^+$ vessels were similar between lean and obese ZSF1 rats at all the time points (see Supplementary material online, Figure S3).

In conclusion, pericyte loss and increased endothelial junctional remodelling are early microvascular events in the development of HFpEF. This dysfunction is restricted to the capillary vasculature devoid of smooth muscle cells, which is consistent with previous reports.²⁶

Pericyte loss leads to diastolic dysfunction

The ZSF1 rat has previously been shown to be a valuable model for studying HFpEF,^{14,15,16} but the multifactorial effects of the metabolic syndrome make it difficult to prove causality of pericyte loss in driving diastolic dysfunction. Therefore, we switched to a model of pericyte loss without external comorbidities. We hypothesized that chronic pericyte loss will lead to a recapitulation of some aspects of the ZSF1 cardiac phenotype. To investigate this, we used mice that carry a mutation within the PDGF-B retention motive ($PDGF\text{-B}^{\text{ret/ret}}$), such that PDGF-B does not bind the extracellular matrix around endothelial cells and can diffuse away.^{19,27} This results in a reduced pericyte recruitment in the capillary wall, leading to a drop in pericyte coverage, previously described in the eye and brain.^{18,19,28} Previous characterizations of these animals’ cardiac phenotype are limited, male $PDGF\text{-B}^{\text{ret/ret}}$ mice have shown eccentric cardiac remodelling in response to increased aortic stiffness,²⁹ but no studies have investigated how chronic pericyte loss affects diastolic function. We confirmed $PDGF\text{-B}^{\text{ret/ret}}$ mice showed a reduction in pericyte coverage in the heart microvasculature (see Supplementary material online, Figure S4), while showing no change in density of larger cardiac $\alpha\text{-SMA}^+$ vessels (see Supplementary material online, Figure S5A–D).

To understand the development of the cardiac phenotype, both female and male $PDGF\text{-B}^{\text{ret/ret}}$ mice were studied at the age of 12 and 27 weeks (see Supplementary material online, Tables S3 and S4). Female



PDGF-B^{ret/ret} mice showed an increased E/E' at 27 weeks, as well as a significant decrease in IVRT while E/A was unchanged and EF was preserved (Figure 4A–D). This was accompanied by increased heart weight (Figure 4E) and increased immune cell infiltration at 12 weeks, the latter being resolved by 27 weeks (Figure 4F). Since pericyte loss would be systemic, we investigated whether blood pressure was altered. We found no changes in either systolic or diastolic blood

pressure levels (see [Supplementary material online, Figure S5E–H](#)). In contrast to their heart weight, *PDGF-B^{ret/ret}* mice show only a slight increase in cardiomyocyte cross-sectional area (Figure 4G and H), possibly indicating that the increase in heart weight occurred due to oedema. Finally, female *PDGF-B^{ret/ret}* mice displayed increased levels of total cardiac fibrosis at 27 weeks, implying an increase in cardiac stiffness (Figure 4I and J). Female *PDGF-B^{ret/ret}* mice showed a reduction in

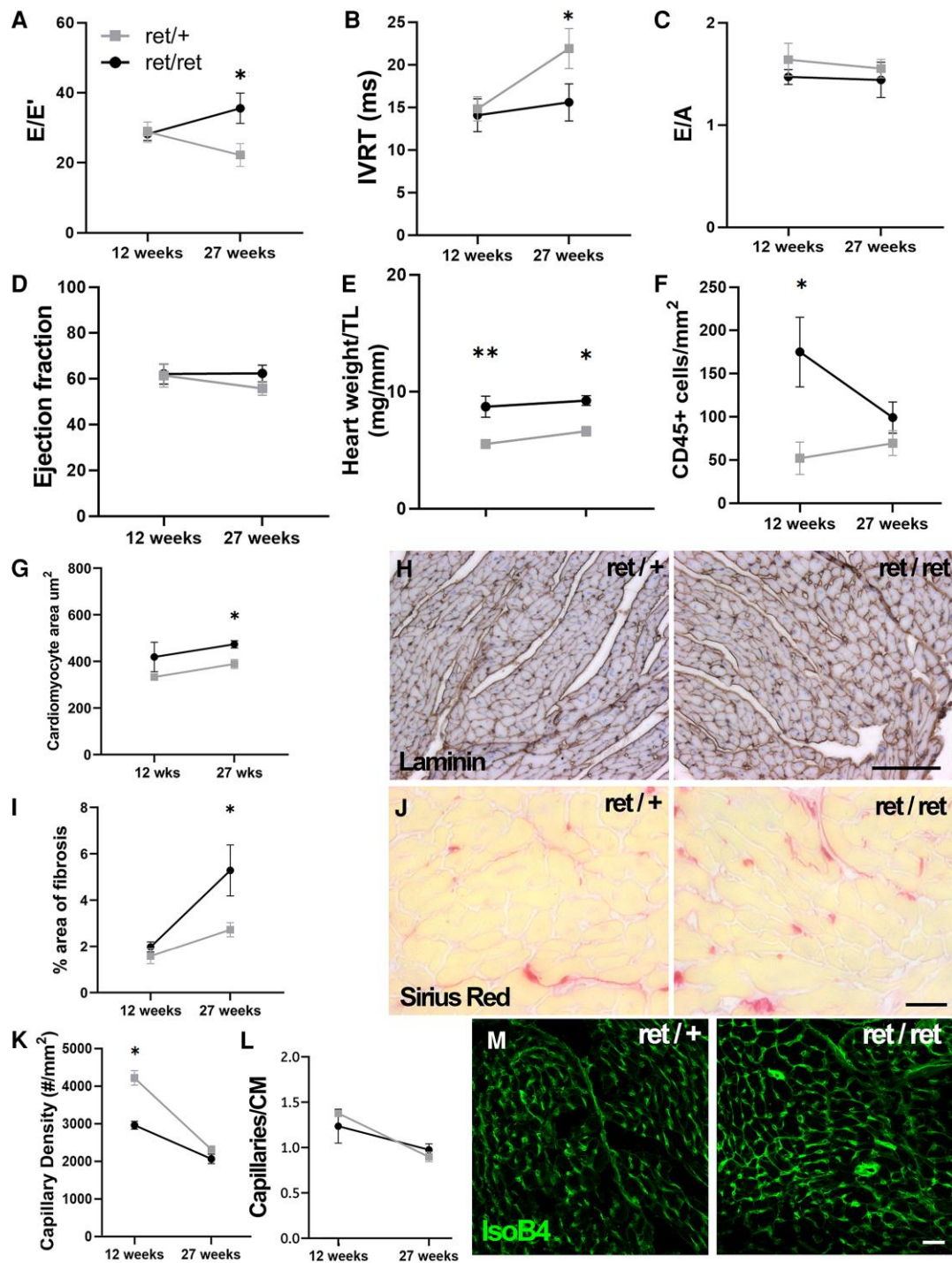


Figure 4 Twenty-seven-week-old female *PDGF-B^{ret/ret}* mice show echocardiographic signs of diastolic dysfunction and cardiac fibrosis. Diastolic function was assessed using E/E' ratio (A), isovolumetric relaxation time (B), E/A (C) while normal systolic function is shown with the preserved ejection fraction (D). The heart weight to tibia length was evaluated as a sign of hypertrophy (E). Cardiac CD45 staining was used to measure immune cell infiltration (F). Cardiac laminin staining was used to measure cardiomyocyte cross-sectional area (G and H). Cardiac Sirius Red staining was used to assess the presence of total fibrosis (I and J). Capillary density of *PDGF-B^{ret/ret}* 12-week- and 27-week-old mice was assessed via isolectinB4 staining (K and M) and also normalized to cardiomyocyte size to give the average number of capillaries per cardiomyocyte (L). Representative images are at 27 weeks. Scale bars are 30 μm (H and M) and 50 μm (J) and apply to all images within a panel. $n = 3$ *ret/+* and 5 *ret/ret* at 12 weeks and $n = 9$ *ret/+* and 9 *ret/ret* at 27 weeks, for *PDGF-B^{ret/+}* and *PDGF-B^{ret/ret}*, respectively. Values are presented as mean \pm SEM. Significance is assessed by a non-paired two-way analysis of variance followed by Sidak's multiple comparisons test with * $P < 0.05$, ** $P < 0.01$, and *** $P < 0.001$. CM, cardiomyocyte; E, early mitral inflow peak velocity; E' , early diastolic annulus peak velocity; EF, ejection fraction; HW heart weight; IsoB4, isolectinB4; IVRT, isovolumetric relaxation time; PDGF-B, platelet-derived growth factor B; TL, tibia length.

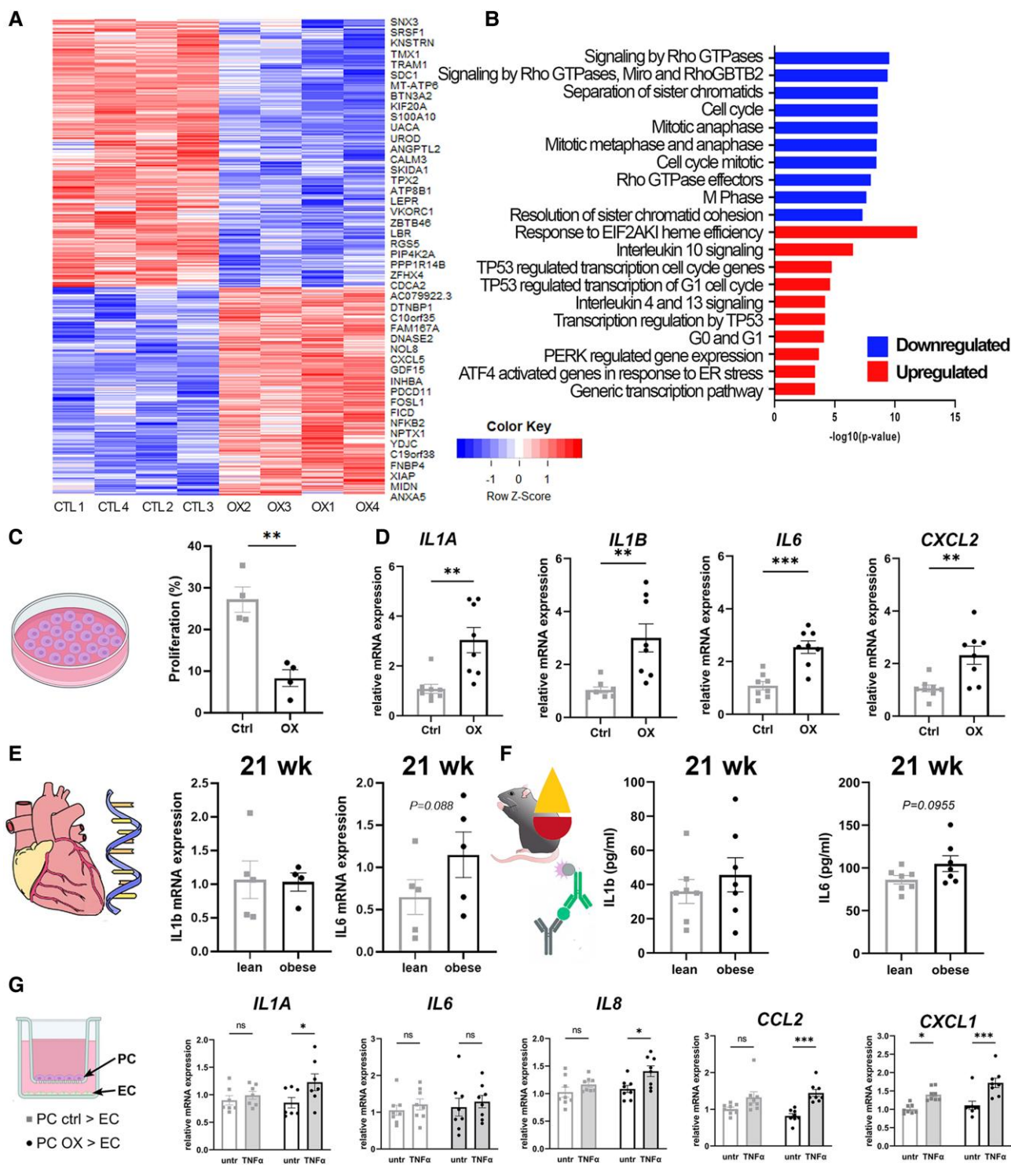


Figure 5 Pericytes exposed to oxidative stress are more inflammatory and make endothelial cells more reactive to inflammatory signals. Human pericytes were exposed to oxidative stress ($100 \mu\text{M H}_2\text{O}_2$) for 24 h. Four replicates per condition were processed for bulk RNA-seq followed by Reactome pathway analysis on the differentially expressed genes. Hierarchical clustering and heatmaps of upregulated and downregulated differentially expressed genes (2619 differentially expressed genes, adjusted $P < 0.05$) after oxidative stress (OX) vs. non-oxidative conditions (CTL) (A). The scale bar represents the gene expression difference between the maximum and minimum values for each gene by z-score. Graphs represent the top 10 enriched pathways associated with downregulated (blue) and upregulated (red) genes in oxidative stress-treated pericytes vs. controls (B). Multiple cell cycle pathways were overrepresented in genes downregulated by oxidative stress vs. controls, whereas p53-mediated cell cycle arrest, ER stress, and interleukins pathways were enriched in genes upregulated by oxidative stress vs. controls. Pericytes treated with oxidative stress for 24 h show reduced proliferation as assessed by a Ki67 staining (C). Pericytes treated with oxidative stress for 24 h upregulate the expression of interleukin-1 alpha, interleukin-1 (continued)

capillary density at 12 weeks; however, no difference was observed at 27 weeks (Figure 4K–M). Furthermore, when average number of capillaries per cardiomyocyte was calculated, no difference was observed (Figure 4L). Male *PDGF-B^{ret/ret}* showed a similar phenotype in many aspects (i.e. increased heart weight, increased CD45+ immune cell infiltration) but had limited characteristics of diastolic dysfunction such that they did not show altered *E/E'*, increased cardiomyocyte hypertrophy, or increased fibrosis (see [Supplementary material online, Figure S6](#)). These data indicate the presence of diastolic dysfunction at least in the female mice, with some possible eccentric cardiac remodelling. The latter is likely due to a decrease in peripheral resistance without an increase in blood pressure. Though the mice have dysfunction during diastole, there are no indications that the heart is failing.

Pericyte dysfunction drives increased inflammation in the endothelium

We have shown that a metabolic syndrome-associated model of pre-HFpEF is associated with pericyte loss and that pericyte loss alone can lead to many aspects of diastolic dysfunction, but how comorbidities affect pericyte function is not known. We therefore exposed human pericytes *in vitro* to oxidative stress (OX; 100 μ M H₂O₂) and performed bulk RNA-seq to identify the transcriptional signatures of dysfunctional pericytes vs. healthy cells. The gene expression patterns between the OX-treated condition and control cells (Figure 5A and B) were markedly different but similar between each replicate from the same condition. The downregulated genes in OX vs. controls were associated with multiple cell cycle pathways, whereas p53-mediated cell cycle arrest, ER stress, and interleukin pathways were enriched in genes upregulated by OX vs. controls (Figure 5A and B). We further confirmed that pericyte proliferation was reduced after OX treatment by a Ki67 staining (Figure 5C). This analysis indicates that pericyte dysfunction induced by oxidative stress is associated with impaired proliferation, confirming our findings that pericytes *in vivo* are less proliferative (Figure 3A and B).

Microvascular dysfunction leading to chronic inflammation is central to the current dogma of how HFpEF develops.² In the brain, pericytes are active neuroinflammatory cells, producing cytokines such as interleukins and chemokines in response to inflammatory signals.³⁰ We, therefore, investigated whether the mechanism by which the loss of pericytes could induce diastolic dysfunction was by altering immune signalling in the heart. We assessed cytokine production by the pericytes exposed to oxidative stress by qPCR. In agreement with our RNA-seq results (Figure 5A), we found upregulations in IL1A, IL1B, IL6, and C-X-C motif chemokine ligand 2 (Figure 5D). We next assessed cytokine expression in the hearts of 14- and 21-week-old ZSF1 rats by qPCR. We found a trend to an increase in IL6 mRNA expression in the obese rats vs. lean but no difference in IL1B expression at 21 weeks (Figure 5E). No differences in either were observed at 14 weeks (data not shown). Though observed changes in expression were small, this represents whole heart RNA and therefore would indicate some cell

types have higher changes in expression. Looking at the circulating levels of these proteins in the ZSF1 rats, we also found that levels of IL6, but not IL1B, are slightly increased in the ZSF1 obese rats at 21 weeks (Figure 5F), though the difference is not statistically significant.

We then investigated the effect of this upregulation in pericyte cytokine production on endothelial cells. To test this, pericytes were treated with oxidative stress for 24 h and then co-cultured with endothelial cells using a transwell system where pericytes and endothelial cells do not make direct contact (Figure 5G). Pericytes and endothelial cells were co-incubated for 2 days before exposure to low levels of TNF α (1 ng/mL for 8 h) that would normally not induce much inflammation in endothelial cells. Accordingly, control pericyte–endothelial co-cultures did not result in significant gene upregulation in endothelial cells in response to TNF α (Figure 5G). In contrast, endothelial cells co-cultured with OX-treated pericytes upregulated *IL1A*, *IL8*, *CCL2*, and *CXCL1* (Figure 5G).

Discussion

Here, using the ZSF1 obese rat as a pre-HFpEF model, we report that microvascular dysfunction and pericyte loss precede the development of diastolic dysfunction. Using the *PDGF-B^{ret/ret}* mice, a model that allows us to study the role of pericytes in the absence of external comorbidities, we show that pericyte loss alone leads to some aspects of diastolic dysfunction and can cause most of the histological changes associated with left ventricular diastolic dysfunction. Our data support a mechanism whereby cardiac pericyte loss is, at least partially, caused by cell cycle arrest and leads to functional impairment of the microvasculature. Pericyte dysfunction was associated with adverse endothelial junction remodelling and increased capillary luminal diameter. Functionally, we show that pericytes exposed to oxidative stress exhibit an inflammatory profile that sensitizes endothelial cells to inflammation. We propose that this triggers and/or amplifies the downstream cascades of microvascular dysfunction driving myocardial remodelling in HFpEF. Our findings significantly change the current understanding of how HFpEF develops, highlighting that microvascular endothelial dysfunction, previously proposed to drive HFpEF,² is at least partially the result of comorbidity-induced pericyte dysfunction. Pericytes have previously been shown to be vulnerable to HFpEF-associated risk factors, including obesity, hyperlipidaemia, hyperglycaemia, and type 2 diabetes mellitus, and the associated oxidative stress.^{31,32,33,34,35,36} Altogether, we provide evidence that pericyte dysfunction plays an early and causal role in diastolic dysfunction and should no longer be considered as a bystander effect secondary to endothelial dysfunction. Rather, we propose that pericytes amplify the chronic inflammation that leads to HFpEF development.

Despite being an abundant cell type in the heart,³⁷ little is known about the role of pericytes in this organ, though they have been significantly studied in the brain,²⁸ kidney,³⁸ and retina.³⁹ During development, pericyte loss leads to micro-haemorrhages and oedema in the mouse embryo.¹⁹ Pericytes also prevent capillary rarefaction in some disease states.¹⁷ In the kidney, pericyte ablation using a genetic model

Figure 5 Continued

beta, interleukin 6, and C-X-C motif chemokine ligand 2 (B, *n* = 8) (D). Quantitative polymerase chain reaction on the hearts of 21-week-old obese and lean ZSF1 rats for interleukin-1 beta and interleukin 6 (E). Detection of circulating levels of interleukin-1 beta and interleukin 6 in plasma of lean and obese ZSF1 rats at 21 weeks by ELISA (F). Oxidative stress-treated and control pericytes were co-cultured with endothelial cells for 2 days and then treated with TNF α (1 ng/mL for 8 h) (G). Low TNF α concentration was chosen such that they did not induce inflammation in control conditions. Endothelial cells cultured with oxidative stress-treated pericytes upregulated interleukin-1 alpha, interleukin 8, C-C motif chemokine ligand 2, and C-X-C motif chemokine ligand 1 (G, *n* = 8 per condition). Values are presented as mean \pm SEM. Significance is assessed by an unpaired Student's *t*-test (C–F) or a two-way analysis of variance (G) with Sidak's *post hoc* test with **P* < 0.05, ***P* < 0.01, and ****P* < 0.001. CCL2, C-C motif chemokine ligand 2; CXCL1, C-X-C motif chemokine ligand 1; CXCL2, C-X-C motif chemokine ligand 2; EC, endothelial cell; IL1A, interleukin-1 alpha; IL1B, interleukin-1 beta; IL6, interleukin 6; IL8, interleukin 8; OX, oxidative stress; PC, pericyte.

led to a decrease in the density of smaller vessels (diameter < 15 μm).⁴⁰ Several brain disorders are characterized by pericyte loss, and genetically induced pericyte deficiency leads to microvascular regression and increased blood–brain barrier (BBB) permeability.¹⁸ Moreover, pericyte deficiency directly impacts endothelial cell behaviour and function with consequences for the BBB integrity.⁴¹ There is also growing evidence that pericytes constitute a progenitor pool for other mural/support cells, the loss of which would hamper the repair of and response to comorbidity-induced damage.¹⁸

The fact that female *PDGF-B^{ret/ret}* mice exhibited severe cardiac pericyte loss and diastolic dysfunction associated with cardiomyocyte hypertrophy, increased fibrosis and early infiltration of immune cells, is novel and important, implicating pericyte dysfunction as an important driver of diastolic dysfunction. At the same time, both female and male *PDGF-B^{ret/ret}* mice showed an increase in end-diastolic volume while the increase in cardiomyocyte cross-sectional area was less pronounced in the males, suggesting eccentric hypertrophy. This can be explained by the increase in stroke volume that, in the absence of increased peripheral resistance, leads to increased end-diastolic volume and eccentric remodelling. The sexual dimorphism in the *PDGF-B^{ret/ret}* mice is of interest with respect to the human presentation of HFpEF. Indeed, female sex is a risk factor for HFpEF, and increased prevalence in post-menopausal women is well documented.⁴² Moreover, female sex has been shown to be independently associated with the presence of diastolic dysfunction and worse clinical outcomes in a cohort of elderly patients with HFpEF.⁴³ Interestingly, a recent study found sex differences in the relationship between microvascular dysfunction in the skin and HFpEF risk.⁴⁴ This study found that impaired microvascular responses in the skin were associated with a higher risk of HFpEF in women with type 2 diabetes but not in men. The *PDGF-B^{ret/ret}* mice have previously been shown to develop kidney failure.¹⁹ Patients with chronic kidney disease (CKD) are at risk of developing HFpEF.⁴⁵ Therefore, it is difficult, in this model, to differentiate between the kidneys causing HF or the pericyte defects causing both HF and CKD. This is further highlighted by the fact that pericyte dysfunction has been implicated in renal fibrosis that leads to CKD.^{38,46} Pericytes are also important in controlling vascular permeability.⁸ Discrepancies between the cardiomyocyte hypertrophy and heart weight in the *PDGF-B^{ret/ret}* mice hinted that oedema may have been present. Furthermore, the ZSF1 rats showed increased gap width between endothelial cells, which often indicates increased permeability. But given that we had not measured oedema itself in the ZSF1 rats, we did not pursue this further. We therefore cannot rule out a significant role for vascular leakage in the development of the phenotype. Pericytes are susceptible to oxidative stress⁴⁷; however, previous studies focused on pericyte apoptosis and not pericyte–endothelial cell crosstalk. We show for the first time that dysfunctional pericytes exposed to oxidative stress can prime endothelial cells to inflammatory signals, propagating an inflammatory cascade within the microvasculature. Of course, our *in vitro* experiments do not fully capture the *in vivo* situation. *In vivo*, a portion of pericytes disappears while the remaining ones are dysfunctional (i.e. altered morphology), which is difficult to mimic *in vitro*. Pericyte loss may be attributed to pericyte detachment and/or apoptosis, though we did not measure this directly *in vivo*. Dying cells are known to release cytokines that can trigger inflammation in neighbouring cells, via a mechanism called cell death-mediated cytokine release and cytokine-regulated apoptosis-induced apoptosis. Nevertheless, this finding elevates pericytes from structural cells of the vascular wall to paracrine sensors of the microvascular microenvironment and highlights the importance of thinking of the microvasculature as a complete unit and not just as individual cell types.

In conclusion, we propose that the loss of pericytes contributes to HFpEF by accentuating endothelial inflammation. Indeed, we suggest a mechanism by which oxidative stress can drive pericyte dysfunction, and pericyte loss or dysfunctional pericytes produce cytokines that make endothelial cells hypersensitive to inflammatory signals.

Nitrosative stress created by immune cells has been shown to be essential for HFpEF development,⁴⁸ but here, we propose that the pericyte loss and dysfunction are sufficient to initiate the inflammatory phenotype. To date, the only treatment showing any efficacy against HFpEF is the sodium–glucose cotransporter-2 (SGLT2) inhibitors.⁴⁹ However, the SGLT2 inhibitor empagliflozin improves cardiac function and reduces hospitalization but does not cure the disease. The fact that pericytes are a highly proliferative cell type with a strong turnover rate indicates that they may be more easily targeted therapeutically, as compared with cardiomyocytes that are terminally differentiated. The fact that pericytes replenish themselves means that the loss should be reversible. Interestingly, a recent paper highlighted the possibility of reversing pericyte loss in diabetic mice with retinopathy using inhibitors of soluble epoxide hydrolase and such a strategy may also work in the heart.⁵⁰

Lead author biography



Ilona Cuijpers did a joint PhD between KU Leuven and the University of Maastricht, successfully defending her thesis in 2020. Her thesis work focused on HFpEF, where she studied the ZSF1 rat model as well as studying the role of fibrosis. She was involved in several European consortium and worked to organize interaction and collaboration between the partners. After graduating, she joined MedPace working on coordination of clinical trials.



Mandy Grootaert obtained her PhD in 2016 from the University of Antwerp where she investigated the role of cell death and autophagy in atherosclerosis. Her deep interest in cardiovascular ageing led her to her first post-doc position at the lab of Prof. Bennett at the University of Cambridge, where she studied cell senescence in vascular smooth muscle cells. In August 2021, she joined the lab of Prof. Jones at KU Leuven to study microvascular dysfunction in diastolic heart failure. Since September 2023, she is appointed as an Assistant Professor at UCLouvain where she will continue to work on cardiometabolic diseases.



During his doctorate at the University of Bristol, Steven J. Simmonds studied the role of the Wnt signaling pathway in macrophage foam cell formation and its implication for atherosclerosis. After successfully defending his thesis, he relocated to the KU Leuven and has gone on to study the cellular and molecular pathways underpinning heart failure with preserved ejection fraction. Outside of research, Steven is engaged in many projects, such as the Pint of Science festival, designed to increase the interaction between scientific researchers, the public, and policymakers.

tween scientific researchers, the public, and policymakers.

Supplementary material

Supplementary material is available at *European Heart Journal Open* online.

Data availability

All data available upon request.

Acknowledgements

We would like to thank Cecilia Ohlsson and Christer Betsholtz for providing cohorts of *PDGF-B^{ret/ret}* mice and littermate controls from this study, Prof. P. Herijgers for providing the non-invasive CODA tail-cuff system, and Bram Callewaert, Liene Vertommen, Caroline Walschap, and Ümare Col for the assistance in the lab. The graphical abstract was created with BioRender.com.

Funding

We acknowledge the support of Fonds voor Wetenschappelijk Onderzoek (1160718N to I.C. and G091018N and G0B5920N to E.A.V.J. and S.H. GOH7716N and GOH7220N to EAVJ). We acknowledge the support of the European Union's Horizon 2020 research and innovation programme through the project CRUCIAL (848109 to E.A.J.V.). DFG (HA 7512/2-1 and HA 7512/2-4 to N.H.) European Union's Horizon 2020 research and innovation program under grant agreement no. 739593 to N.H. and InnovationsFoRUM IF-023-22 and IF-034-22.

Conflict of interest: None.

References

- Borlaug BA, Paulus WJ. Heart failure with preserved ejection fraction: pathophysiology, diagnosis, and treatment. *Eur Heart J* 2011;**32**:670–679.
- Paulus WJ, Tschope C. A novel paradigm for heart failure with preserved ejection fraction: comorbidities drive myocardial dysfunction and remodeling through coronary microvascular endothelial inflammation. *J Am Coll Cardiol* 2013;**62**:263–271.
- Sinha A, Rahman H, Webb A, Shah AM, Perera D. Untangling the pathophysiological link between coronary microvascular dysfunction and heart failure with preserved ejection fraction. *Eur Heart J* 2021;**42**:4431–4441.
- Rush CJ, Berry C, Oldroyd KG, Rocchiccioli JP, Lindsay MM, Touyz RM, Murphy CL, Ford TJ, Sidik N, McEntegart MB, Lang NN, Jhund PS, Campbell RT, McMurray JJV, Petrie MC. Prevalence of coronary artery disease and coronary microvascular dysfunction in patients with heart failure with preserved ejection fraction. *JAMA Cardiol* 2021;**6**:1130–1143.
- Ahmad A, Corban MT, Toya T, Verbrugge FH, Sara JD, Lerman LO, Borlaug BA, Lerman A. Coronary microvascular dysfunction is associated with exertional haemodynamic abnormalities in patients with heart failure with preserved ejection fraction. *Eur J Heart Fail* 2021;**23**:765–772.
- Taqueti VR, Solomon SD, Shah AM, Desai AS, Groarke JD, Osborne MT, Hainer J, Bibbo CF, Dorbala S, Blankstein R, Di Carli MF. Coronary microvascular dysfunction and future risk of heart failure with preserved ejection fraction. *Eur Heart J* 2018;**39**:840–849.
- Mohammed SF, Hussain S, Mirzoyev SA, Edwards WD, Maleszewski JJ, Redfield MM. Coronary microvascular rarefaction and myocardial fibrosis in heart failure with preserved ejection fraction. *Circulation* 2015;**131**:550–559.
- van Splunder H, Villacampa P, Martinez-Romero A, Graupera M. Pericytes in the disease spotlight. *Trends Cell Biol* 2023;S0962-8924(23)00111-3.
- Hartmann DA, Berthiaume AA, Grant RI, Harrill SA, Koski T, Tieu T, McDowell KP, Faino AV, Kelly AL, Shih AY. Brain capillary pericytes exert a substantial but slow influence on blood flow. *Nat Neurosci* 2021;**24**:633–645.
- Hall CN, Reynell C, Gesslein B, Hamilton NB, Mishra A, Sutherland BA, O'Farrell FM, Buchan AM, Lauritzen M, Attwell D. Capillary pericytes regulate cerebral blood flow in health and disease. *Nature* 2014;**508**:55–60.
- Dohgu S, Takata F, Yamauchi A, Nakagawa S, Egawa T, Naito M, Tsuruo T, Sawada Y, Niwa M, Kataoka Y. Brain pericytes contribute to the induction and up-regulation of blood-brain barrier functions through transforming growth factor-beta production. *Brain Res* 2005;**1038**:208–215.
- Kovac A, Erickson MA, Banks WA. Brain microvascular pericytes are immunoreactive in culture: cytokine, chemokine, nitric oxide, and LRP-1 expression in response to lipopolysaccharide. *J Neuroinflammation* 2011;**8**:139.
- Cuijpers I, Carai P, Mendes-Ferreira P, Simmonds SJ, Mulder P, Miranda-Silva D, De Giorgio D, Pokreisz P, Heymans S, Jones EAV. The effect of different anaesthetics on echocardiographic evaluation of diastolic dysfunction in a heart failure with preserved ejection fraction model. *Sci Rep* 2020;**10**:15701.
- Hamdani N, Franssen C, Lourenco A, Falcao-Pires I, Fontoura D, Leite S, Plettig L, López B, Ottenheijm CA, Becher PM, González A, Tschöpe C, Díez J, Linke WA, Leite-Moreira AF, Paulus WJ. Myocardial titin hypophosphorylation importantly contributes to heart failure with preserved ejection fraction in a rat metabolic risk model. *Circ Heart Fail* 2013;**6**:1239–1249.
- Leite S, Oliveira-Pinto J, Tavares-Silva M, Abdellatif M, Fontoura D, Falcao-Pires I, Leite-Moreira AF, Lourenço AP. Echocardiography and invasive hemodynamics during stress testing for diagnosis of heart failure with preserved ejection fraction: an experimental study. *Am J Physiol Heart Circ Physiol* 2015;**308**:H1556–H1563.
- Schauer A, Draskowski R, Jannasch A, Kirchhoff V, Goto K, Mannel A, Barthel P, Augstein A, Winzer E, Tugtekin M, Labeit S, Linke A, Adams V. ZSF1 rat as animal model for HFpEF: development of reduced diastolic function and skeletal muscle dysfunction. *ESC Heart Fail* 2020;**7**:2123–2134.
- Schrimpf C, Teebken OE, Wilhelm M, Duffield JS. The role of pericyte detachment in vascular rarefaction. *J Vasc Res* 2014;**51**:247–258.
- Armulik A, Genove G, Betsholtz C. Pericytes: developmental, physiological, and pathological perspectives, problems, and promises. *Dev Cell* 2011;**21**:193–215.
- Lindblom P, Gerhardt H, Liebner S, Abramsson A, Enge M, Hellstrom M, Backstrom G, Fredriksson S, Landegren U, Nystrom HC, Bergstrom G, Dejana E, Ostman A, Lindahl P, Betsholtz C. Endothelial PDGF-B retention is required for proper investment of pericytes in the microvessel wall. *Genes Dev* 2003;**17**:1835–1840.
- Kamouchi M, Kitazono T, Ago T, Wakisaka M, Kuroda J, Nakamura K, Hagiwara N, Ooboshi H, Ibayashi S, Iida M. Hydrogen peroxide-induced Ca²⁺ responses in CNS pericytes. *Neurosci Lett* 2007;**416**:12–16.
- Walton J. Lead aspartate, an *en bloc* contrast stain particularly useful for ultrastructural enzymology. *J Histochem Cytochem* 1979;**27**:1337–1342.
- Linke WA, Hamdani N. Gigantic business: titin properties and function through thick and thin. *Circ Res* 2014;**114**:1052–1068.
- Winkler EA, Bell RD, Zlokovic BV. Central nervous system pericytes in health and disease. *Nat Neurosci* 2011;**14**:1398–1405.
- Jin Y, Ding Y, Richards M, Kaakinen M, Giese W, Baumann E, Szymborska A, Rosa A, Nordling S, Schimmel L, Akmerić EB, Pena A, Nwadozi E, Jamalpour M, Holstein K, Sáinz-Jaspeado M, Bernabeu MO, Welsh M, Gordon E, Franco CA, Vestweber D, Eklund L, Gerhardt H, Claesson-Welsh L. Tyrosine-protein kinase yes controls endothelial junctional plasticity and barrier integrity by regulating VE-cadherin phosphorylation and endocytosis. *Nature Cardiovascular Research* 2022;**1**:1156–1173.
- Bentley K, Franco CA, Philippides A, Blanco R, Dierkes M, Gebala V, Stanchi F, Jones M, Aspalter IM, Cagna G, Westrom S, Claesson-Welsh L, Vestweber D, Gerhardt H. The role of differential VE-cadherin dynamics in cell rearrangement during angiogenesis. *Nat Cell Biol* 2014;**16**:309–321.
- Waddingham MT, Sonobe T, Tsuchimochi H, Edgley AJ, Sukumaran V, Chen YC, Hansra SS, Schwenke DO, Umetani K, Aoyama K, Yagi N, Kelly DJ, Gaderi S, Herwig M, Kolijn D, Mügge A, Paulus WJ, Ogo T, Shirai M, Hamdani N, Pearson JT. Diastolic dysfunction is initiated by cardiomyocyte impairment ahead of endothelial dysfunction due to increased oxidative stress and inflammation in an experimental prediabetes model. *J Mol Cell Cardiol* 2019;**137**:119–131.
- Ostman A, Andersson M, Betsholtz C, Westermark B, Heldin CH. Identification of a cell retention signal in the B-chain of platelet-derived growth factor and in the long splice version of the A-chain. *Cell Regul* 1991;**2**:503–512.
- Armulik A, Genove G, Mae M, Nisancioglu MH, Wallgard E, Niaudet C, He L, Norlin J, Lindblom P, Strittmatter K, Johansson BR, Betsholtz C. Pericytes regulate the blood-brain barrier. *Nature* 2010;**468**:557–561.
- Nystrom HC, Lindblom P, Wickman A, Andersson I, Norlin J, Faldt J, Lindahl P, Skott O, Bjarnegård M, Fitzgerald SM, Caidahl K, Gan LM, Betsholtz C, Bergström G. Platelet-derived growth factor B retention is essential for development of normal structure and function of conduit vessels and capillaries. *Cardiovasc Res* 2006;**71**:557–565.
- Jansson D, Rustenhoven J, Feng S, Hurley D, Oldfield RL, Bergin PS, Mee EW, Faull RL, Dragunow M. A role for human brain pericytes in neuroinflammation. *J Neuroinflammation* 2014;**11**:104.
- Warmke N, Griffin KJ, Cubbon RM. Pericytes in diabetes-associated vascular disease. *J Diabetes Complications* 2016;**30**:1643–1650.
- Tucsek Z, Toth P, Tarantini S, Sosnowska D, Gautam T, Warrington JP, Giles CB, Wren JD, Koller A, Ballabh P, Sonntag WE, Ungvari Z, Csiszar A. Aging exacerbates obesity-induced cerebrovascular rarefaction, neurovascular uncoupling, and cognitive decline in mice. *J Gerontol A Biol Sci Med Sci* 2014;**69**:1339–1352.
- Zechariah A, ElAli A, Hagemann N, Jin F, Doeppner TR, Helfrich I, Mies G, Herrmann DM. Hyperlipidemia attenuates vascular endothelial growth factor-induced angiogenesis, impairs cerebral blood flow, and disturbs stroke recovery via decreased pericyte coverage of brain endothelial cells. *Arterioscler Thromb Vasc Biol* 2013;**33**:1561–1567.
- Shah GN, Price TO, Banks WA, Morofuji Y, Kovac A, Ercal N, Sorenson CM, Shin ES, Sheibani N. Pharmacological inhibition of mitochondrial carbonic anhydrases protects mouse cerebral pericytes from high glucose-induced oxidative stress and apoptosis. *J Pharmacol Exp Ther* 2013;**344**:637–645.
- Nwadozi E, Rudnicki M, Haas TL. Metabolic coordination of pericyte phenotypes: therapeutic implications. *Front Cell Dev Biol* 2020;**8**:77.
- Geraldes P, Hiraoka-Yamamoto J, Matsumoto M, Clermont A, Leitges M, Marette A, Aiello LP, Kern TS, King GL. Activation of PKC-delta and SHP-1 by hyperglycemia causes vascular cell apoptosis and diabetic retinopathy. *Nat Med* 2009;**15**:1298–1306.

37. Nees S, Weiss DR, Senftl A, Knott M, Forch S, Schnurr M, Weyrich P, Juchem G. Isolation, bulk cultivation, and characterization of coronary microvascular pericytes: the second most frequent myocardial cell type in vitro. *Am J Physiol Heart Circ Physiol* 2012;**302**:H69–H84.
38. Lin SL, Kisseleva T, Brenner DA, Duffield JS. Pericytes and perivascular fibroblasts are the primary source of collagen-producing cells in obstructive fibrosis of the kidney. *Am J Pathol* 2008;**173**:1617–1627.
39. Hammes HP, Lin J, Renner O, Shani M, Lundqvist A, Betsholtz C, Brownlee M, Deutsch U. Pericytes and the pathogenesis of diabetic retinopathy. *Diabetes* 2002;**51**:3107–3112.
40. Kramann R, Wongboonsin J, Chang-Panesso M, Machado FG, Humphreys BD. Gli1(+) pericyte loss induces capillary rarefaction and proximal tubular injury. *J Am Soc Nephrol* 2017;**28**:776–784.
41. Mae MA, He L, Nordling S, Vazquez-Liebanas E, Nahar K, Jung B, Li X, Tan BC, Chin Foo J, Cazenave-Gassiot A, WVenk MR, Zarb Y, Lavina B, Quaggin SE, Jeansson M, Gu C, Silver DL, Vanlandewijck M, Butcher EC, Keller A, Betsholtz C. Single-cell analysis of blood–brain barrier response to pericyte loss. *Circ Res* 2021;**128**:e46–e62.
42. Owan TE, Hodge DO, Herges RM, Jacobsen SJ, Roger VL, Redfield MM. Trends in prevalence and outcome of heart failure with preserved ejection fraction. *N Engl J Med* 2006;**355**:251–259.
43. Sotomi Y, Hikoso S, Nakatani D, Mizuno H, Okada K, Dohi T, Kitamura T, Sunaga A, Kida H, Oeun B, Sato T, Komukai S, Tamaki S, Yano M, Hayashi T, Nakagawa A, Nakagawa Y, Yasumura Y, Yamada T, Sakata Y; PURSUIT-HFpEF Investigators. Sex differences in heart failure with preserved ejection fraction. *J Am Heart Assoc* 2021;**10**:e018574.
44. Canto ED, van Deursen L, Hoek AG, Elders PJM, den Ruijter HM, van der Velden J, van Empel V, Serné EH, Eringa EC, Beulens JWJ. Microvascular endothelial dysfunction in skin is associated with higher risk of heart failure with preserved ejection fraction in women with type 2 diabetes: the Hoorn Diabetes Care System Cohort. *Cardiovasc Diabetol* 2023;**22**:234.
45. Patel N, Yaqoob MM, Aksentijevic D. Cardiac metabolic remodelling in chronic kidney disease. *Nat Rev Nephrol* 2022;**18**:524–537.
46. Chen YT, Chang FC, Wu CF, Chou YH, Hsu HL, Chiang WC, Shen J, Chen YM, Wu KD, Tsai TJ, Duffield JS, Lin SL. Platelet-derived growth factor receptor signaling activates pericyte-myofibroblast transition in obstructive and post-ischemic kidney fibrosis. *Kidney Int* 2011;**80**:1170–1181.
47. Ding X, Zhang M, Gu R, Xu G, Wu H. Activated microglia induce the production of reactive oxygen species and promote apoptosis of co-cultured retinal microvascular pericytes. *Graefes Arch Clin Exp Ophthalmol* 2017;**255**:777–788.
48. Schiattarella GG, Altamirano F, Tong D, French KM, Villalobos E, Kim SY, Luo X, Jiang N, May HI, Wang ZV, Hill TM, Mammen PPA, Huang J, Lee DI, Hahn VS, Sharma K, Kass DA, Lavandro S, Gillette TG, Hill JA. Nitrosative stress drives heart failure with preserved ejection fraction. *Nature* 2019;**568**:351–356.
49. Anker SD, Butler J, Filippatos G, Ferreira JP, Bocchi E, Bohm M, Brunner-La Rocca HP, Choi DJ, Chopra V, Chuquiure-Valenzuela E, Giannetti N, Gomez-Mesa JE, Janssens S, Januzzi JL, Gonzalez-Juanatey JR, Merkely B, Nicholls SJ, Perrone SV, Piña IL, Ponikowski P, Senni M, Sim D, Spinar J, Squire I, Taddei S, Tsutsui H, Verma S, Vinereanu D, Zhang J, Carson P, Lam CSP, Marx N, Zeller C, Sattar N, Jamal W, Schnaidt S, Schnee JM, Brueckmann M, Pocock SJ, Zannad F, Packer M; EMPEROR-Preserved Trial Investigators. Empagliflozin in heart failure with a preserved ejection fraction. *N Engl J Med* 2021;**385**:1451–1461.
50. Hu J, Dziumbila S, Lin J, Bibli SI, Zukunft S, de Mos J, Awwad K, Frömel T, Jungmann A, Devraj K, Cheng Z, Wang L, Fauser S, Eberhart CG, Sodhi A, Hammock BD, Liebner S, Müller OJ, Glaubitz C, Hammes HP, Popp R, Fleming I. Inhibition of soluble epoxide hydrolase prevents diabetic retinopathy. *Nature* 2017;**552**:248–252.